Powder Technology 228 (2012) 36–46

Contents lists available at SciVerse ScienceDirect

Powder Technology

journal homepage: www.elsevier.com/locate/powtec

Application of iron-based powders in tungsten inert gas welding for 17Cr–10Ni–2Mo alloys

Kuang-Hung Tseng *, Ko-Jui Chuang

Institute of Materials Engineering, National Pingtung University of Science and Technology, Pingtung 91201, Taiwan

ARTICLE INFO

Article history:
Received 28 March 2012
Received in revised form 23 April 2012
Accepted 27 April 2012
Available online 11 May 2012

Keywords:
17Cr–10Ni–2Mo alloy
Activated TIG welding
Iron-based compound
Flux powder

ABSTRACT

This study investigates the influences of specific flux powders, including FeF_2, FeO, and FeS on the surface appearance, geometric shape, angular distortion, hot crack susceptibility, and metallurgical properties of 5-mm-thick 17Cr–10Ni–2Mo alloys welded using the tungsten inert gas (TIG) process. Results indicate that TIG welding with FeF_2 powder produces a weld of satisfactory appearance. TIG welding with FeO and FeS powders results in a substantial increase in both the joint penetration and weld aspect ratio, thereby reducing angular distortion of the weldment. TIG welding with FeO and FeS powders increases the delta-ferrite content and decreases welding heat input, and tends to reduce hot crack susceptibility of the welds. This study demonstrates that the application of activated powder assisted TIG welding can improve the weldment performances.

1. Introduction

The TIG welding technique produces high-quality welds in nearly all metals and alloys (except for alloys with a very low melting point). However, TIG welding also has some disadvantages, including the limited thickness of the base metals that can be welded in a single-pass procedure, large heat-to-heat variations in the penetration of the welds, and relatively low productivity gains [1–5]. The low efficiency and productivity of TIG welding can be traced to low welding speeds and a greater number of passes required to fill the groove joint for thick plates or heavy wall pipes. Additional filler metals may also be needed. Edge preparation involves additional costs and requires a substantially longer welding time. These issues detract considerably from the attractiveness of TIG welding.

Developing cost-effective TIG welding techniques will be a key competitive challenge for manufacturers in the future. The most effective manner of increasing the penetration of TIG welds is to use inorganic compounds, called activated flux, in a process called activated TIG welding. The activated TIG welding of stainless steels can obtain a penetration of 8 mm in a single-pass weld without the need for edge preparation [6,7]. The activated flux is usually applied as a suspension (powder in solvent), whereby a thin layer of activated flux can be deposited on the surface of the base metal prior to welding. Activated TIG welding was first proposed by the E.O. Paton Electric Welding Institute (Ukraine) in the 1950s [8], and interest in this novel welding technique has grown over the last decade.

Fluid flow dominates the transfer of heat in a molten weld pool, and thus, determines the geometric dimensions of the welds. In TIG welding with the DC electrode negative, the fluid flow in a molten weld pool is driven mainly by surface tension, the Lorentz force, buoyancy, and aerodynamic drag. The surface tension of pure liquid metals normally decreases as temperature increases. In other words, pure liquid metals have a negative surface tension gradient ($d\gamma/dT<0$). Fig. 1 presents the various driving forces involved in fluid flow in a molten weld pool and their individual effects on weld profile. A positive surface tension gradient ($d\gamma/dT>0$) and an increase in Lorentz force can improve penetration. Current theory on the influence of activated flux on TIG welds states that the surface-active trace elements in a molten weld pool convert the surface tension gradient from a negative to positive value. Thus, fluid flow is directed inward along the surface of the weld pool and downward toward the bottom, which tends to increase penetration of the welds [9–13]. Lucas and Howse indicated that a redistributed current influences the distribution of heat flux in the arc column, the induced Lorentz force, and the convective heat transfer in a molten weld pool [14,15]. However, data are lacking on the interaction between the physics of the arc column and the chemistry of the weld pool for activated TIG welding, and the mechanisms that sustain this effect.

The literature offers limited data on the composition of the flux powders, yet this information is critical to determine the penetration improvement function of the activated fluxes. Although researchers have published substantial information on the use of oxide powder in the activated TIG welding technique, data on sulfide or fluoride powder remain limited. This information is necessary to determine whether the penetration capability of TIG welding with sulfide or fluoride powder is as effective as that with oxide powder. The

* Corresponding author at: No. 1, Hseuhfu Rd., Neipu, Pingtung 91201, Taiwan. Tel.: +886 8 7703202; fax: +886 8 7740552.
E-mail address: tkh@mail.npust.edu.tw (K-H. Tseng).

0032-5910/$ – see front matter © 2012 Elsevier B.V. All rights reserved.
doi:10.1016/j.powtec.2012.04.047

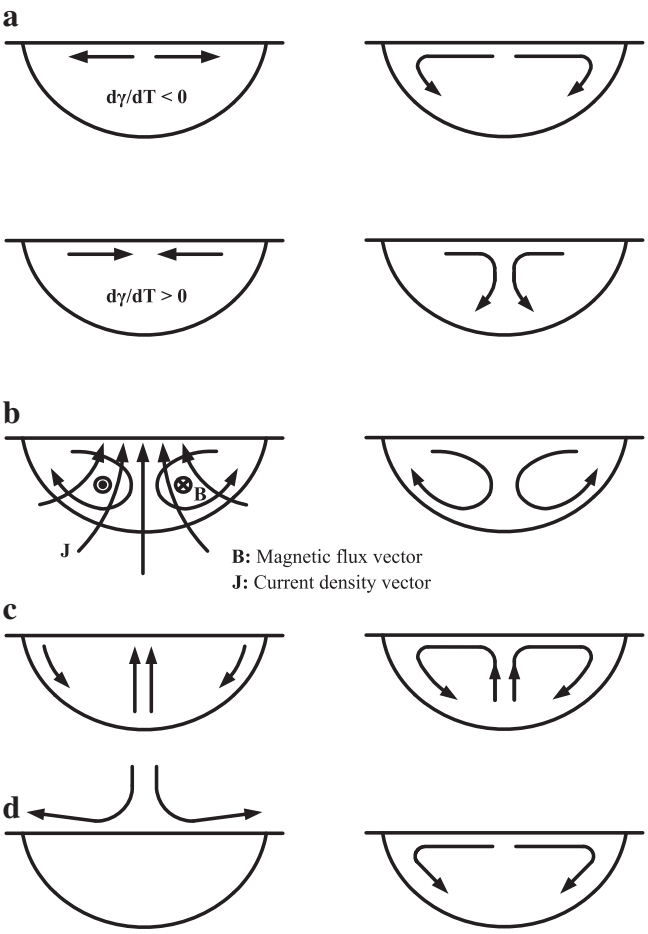

Fig. 1. Driving forces for fluid flow in molten weld pool.

experiments reported in this study used three iron-based compounds to systematically investigate the influence of the flux powders on the surface appearance, geometric shape, angular distortion, hot crack susceptibility, and metallurgical properties of the 17Cr–10Ni–2Mo alloy TIG welds. This study also discusses the interaction model between the arc column and the weld pool for the activated TIG welding process, and compares this with the conventional TIG welding process.

2. Experimental details

The base metal used in this experiment is commercial Fe–17%Cr–10%Ni–2%Mo alloy (austenitic 316 L stainless steel). Table 1 lists the chemical composition of the alloy. The test plates measured 120 × 120 mm, with a thickness of 5 mm. The surface of each specimen was roughly grinded with 240 grit (silicon carbide) flexible abrasive paper to remove all impurities, and was subsequently cleaned with acetone prior to welding. Three iron-based compounds, FeF_2, FeO, and FeS, were used in powdered form (Fig. 2). Table 2 lists the characteristics of the experimental powders. Prior to welding, the powder was mixed with solvent (1500 mg experimental powder was mixed with 1.5 ml methanol) to produce a paint-like consistency, and was subsequently manually applied with a paintbrush as a sufficiently layer thick to prevent visual observation of the base metal beneath. The uniformity of the applied powder flux coating is very important. In the experiments, the thickness of the flux layer and the mean quantity of the flux coating were approximately 0.2 mm and 4.1 mg/cm^2, respectively.

Table 1
Chemical composition (wt.%, balance Fe) of experimental alloy.

C	Si	Mn	P	S	Cr	Ni	Mo	N
0.020	0.47	1.77	0.031	0.002	17.10	10.11	2.05	0.048

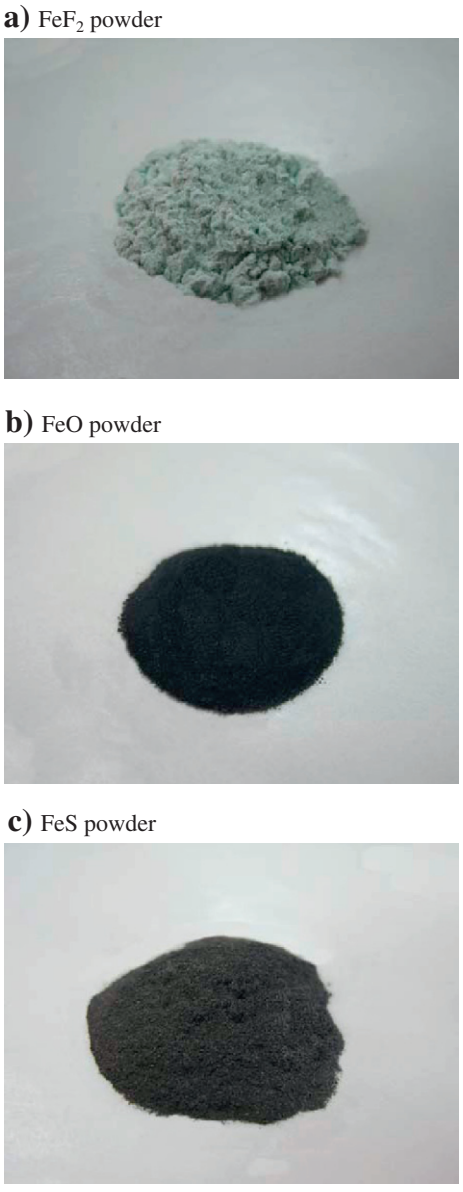

Fig. 2. Original appearance of experimental powders.

Table 2
Characteristic of experimental powders.

Flux powder	FeF_2 powder	FeO powder	FeS powder
Origin	Echo Chemical Co., Ltd.	Echo Chemical Co., Ltd.	Echo Chemical Co., Ltd.
Purity	≥ 99.9%	≥ 99.5%	≥ 99.0%
Molar mass	93.84 g/mol	71.84 g/mol	87.91 g/mol
Density	4.1 g/cm^3	6.0 g/cm^3	4.7 g/cm^3
Melting point	970 °C	1370 °C	1188 °C
Boiling point	1100 °C	3414 °C	decomposes
Lattice energy	2769 kJ/mol	3795 kJ/mol	N/A
Ionization potential	12.5 ± 0.3 eV	8.8 ± 0.2 eV	8.3 ± 0.3 eV

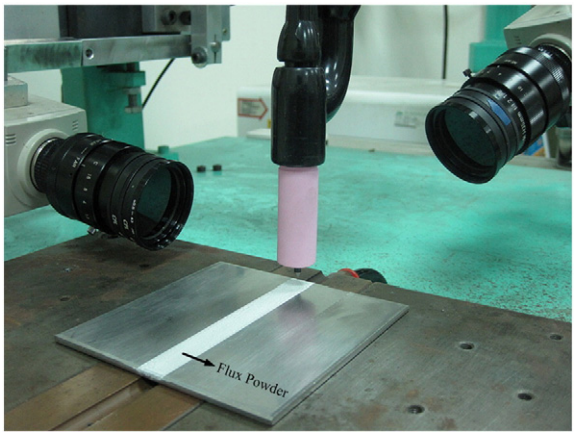

Fig. 3. Experimental setup of TIG welding with flux powder.

The direct current electrode negative (DCEN) mode was used with a mechanized operating system in which the torch traveled at a constant speed. Single-pass, autogenous, bead-on-plate TIG welds were made along the center line of the test specimens. A water-cooled torch with a standard 2% thoriated tungsten electrode rod with a 3.2 mm diameter was used. The electrode tip was a blunt point with a 45° angle. Argon of 99.99% purity was used as shielding gas. The tip angle of the electrode was grounded, and the electrode gap was measured for each new weld prior to welding to ensure that the welding was performed under the same operating conditions. During welding, a charge-coupled device (CCD) detector system was used to observe and record the images of the arc profile. A digital data acquisition system with a sampling rate of 12 samples per second was also used to continuously measure the current and voltage during the experiments. Fig. 3 shows the experimental setup used in this study.

All test specimens were constraint-free during welding to avoid the influence of reaction stresses. Following welding, experiments were conducted to measure the angular distortion in a bead-on-plate welded plate. The angular distortion of the weldment was measured using the mean vertical displacement, as Fig. 4 illustrates. A hole was drilled from the back at points P_1, P_2, and P_3, and a pillar was inserted into each hole. These three pillars (one fixed, two adjustable) were used to adjust the horizontal level, and the distance from each point to the horizontal surface was then recorded. Measurements were taken before and after welding. The differences in measurements before and after welding revealed the vertical displacement caused by welding, and the total angular distortion value θ was derived using the following equation.

$$\theta = 2 \times \tan^{-1} \frac{|(A+B)-(C+D)|}{60} \quad (1)$$

where A, B, C, and D represent the mean vertical displacement values of each point.

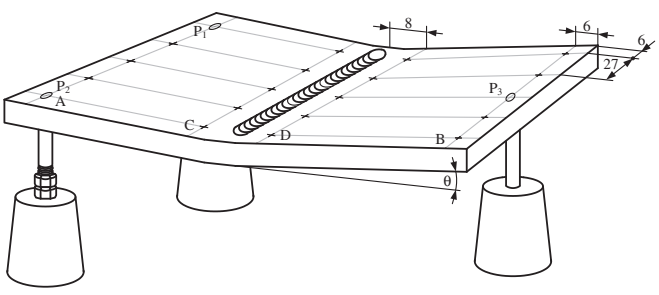

Fig. 4. Schematic diagram of distortion measurement.

Ferrite number (FN) is an arbitrary standardized value designating the ferrite content in the stainless steel weld metals. FN is expected to be approximately equal to the percentage of ferrite in austenitic stainless steel weld metal up to approximately 15%. However, the true percentage of ferrite in the weld metals is overestimated by FN values higher than 15 FN. In this experiment, FN was measured using a calibrated magnetic instrument (ferritoscope). This device detects phases such as ferrite according to the magnetic susceptibility, which differs from that of paramagnetic austenite. To minimize measurement errors resulting from inhomogeneity in the weld metals, the average value of seven measurements from various locations along the as-welded surface was calculated.

The Varestraint (variable restraint) test was used to evaluate the alloy's susceptibility to forming hot crack during welding. This test uses a controlled, rapidly applied bending strain to produce solidification cracks during welding. The welding conditions in this experiment were an arc current of 100 A for 4 s in 3-mm-thick stainless steel sheet, and the arc length was maintained at 1.6 mm. The augmented-tangential strain applied to the surface of specimen was 5%. A spot weld was made in the center of the topside of specimen. The arc was then extinguished and the load immediately applied to force the specimen to conform to the die block. This process produced solidification cracks in both the fusion zone (FZ) and heat-affected zone (HAZ). After testing, the total and maximum crack lengths in the welds were normalized based on the molten weld pool diameter. Fig. 5 shows the Varestraint test method in schematic form.

Vickers microhardness test was used to examine the changes in the mechanical properties and metallurgical structures of weld metal. The hardness distribution profiles across the FZ, HAZ, and partial base metal (BM) were measured under a load of 2.94 N for 15 s.

After welding, the surface appearance and geometric shape of the welds were photographed with a stereomicroscope. The weld geometry in this experiment was characterized using three quality parameters, that is, penetration depth, bead width, and cross-sectional area of the welds. The transverse sections were made at various locations along the welds, whereas samples for metallographic examination were prepared using standard procedures, including sectioning, mounting, grinding, and polishing to a 0.05 μm finish, followed by electrolytic etching in an electrolyte solution consisting of 10 g oxalic acid and 100 ml water. Each sample was examined with a toolmaker's microscope to measure the depth, width, and cross-sectional area of the welds. Each data point represents the average of three samples. Metallurgical characterization of the welds was evaluated using optical microscopy (OM) and scanning electron microscopy (SEM). An X-ray diffractometer with a CuKα radiation source ($\lambda = 0.15418$ nm) was utilized to identify the crystalline of the phases present in weld metal. Furthermore, the diffraction results were used to verify the microstructural observation.

3. Results and discussion

3.1. Prestudy on penetration depth of conventional TIG welds

Penetration depth is a critical quality characteristic of weld geometry. Weld current and travel speed are the primary TIG welding parameters used to determine the penetration depth. The results in Fig. 6 show the measured penetration of autogenous TIG bead-on-plate welds into 5-mm-thick stainless steel as a function of weld current and travel speed. Increasing the weld current increased the penetration depth. The penetration depth is also inversely proportional to travel speed at a particular weld current. For an autogenous TIG welding of stainless steel plate using argon as a shielding gas, the penetration depth achievable in a single-pass without grooving preparation is limited to approximately 3 mm. Increasing the weld current to increase the penetration depth creates an excessively wide weld profile with relatively little gain in penetration, as Fig. 7 shows.

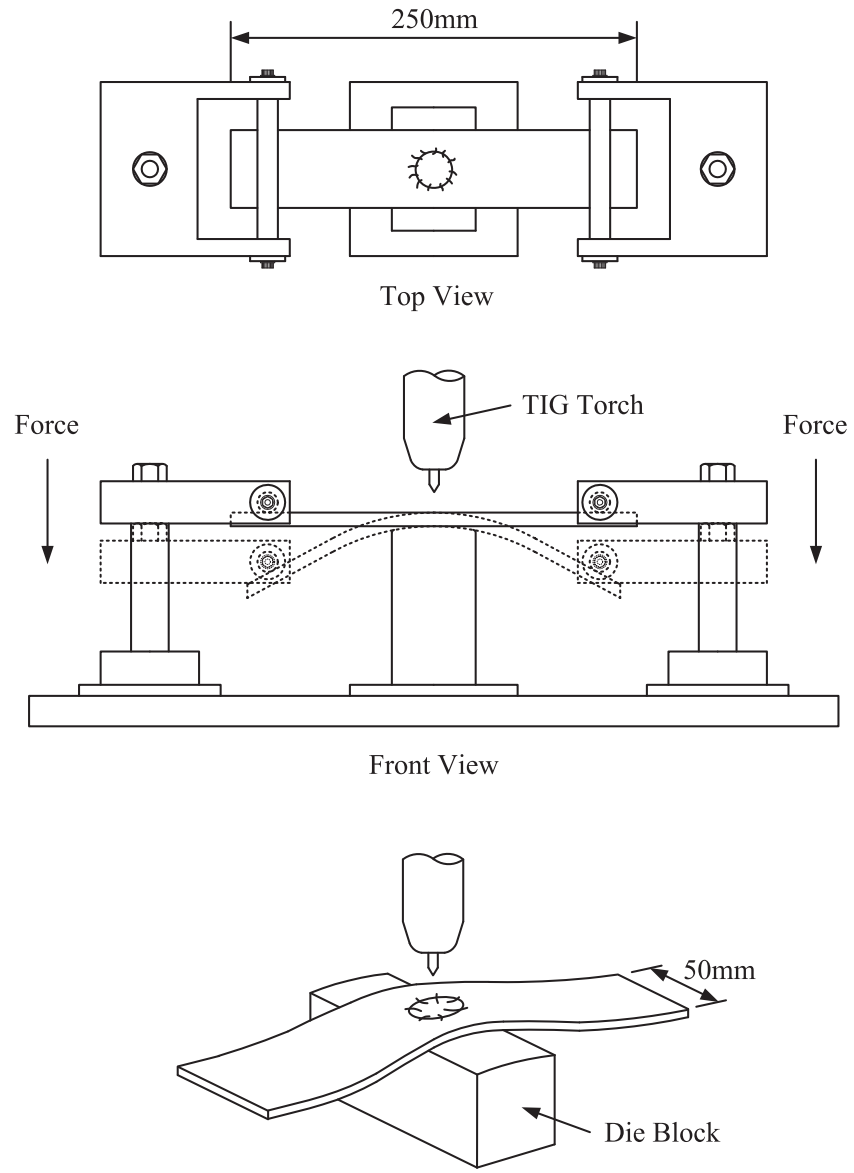

Fig. 5. Schematic diagram of Varestraint test.

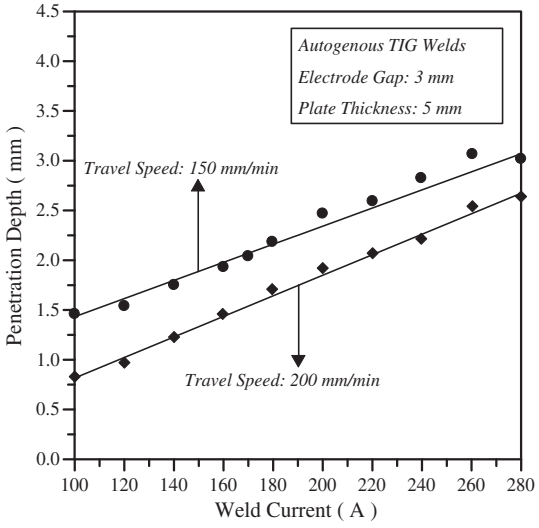

Fig. 6. Effect of process parameters on penetration depth of conventional TIG welds.

3.2. Surface appearance of activated TIG welds

Table 3 lists the process parameter used in the activated TIG welding experiments. Fig. 8 shows the surface appearances of stainless steel TIG welds produced without and with flux powder. Fig. 8a shows the results of TIG welding without flux powder, which produces a smooth, colored surface. Fig. 8b shows that no residual slag and spatter were produced using FeF_2 powder. Fig. 8c shows that FeO powder produced little residual slag and a large amount of spatter. Fig. 8d shows that FeS powder produced excessive residual slag and a small amount of spatter, and the surface is discolored. These results clearly indicate that on stainless steel, FeF_2 powder produces TIG welds with a satisfactory surface appearance, whereas FeO and FeS powders lead to the formation of slag and spatter. Because fluoride compounds have a substantially lower melting point, boiling point, and thermal decomposition temperature than oxide and sulfide compounds, FeF_2 powder is easily melted by the arc heat source of TIG welding. This explains the satisfactory appearance of TIG welds using FeF_2 powder.

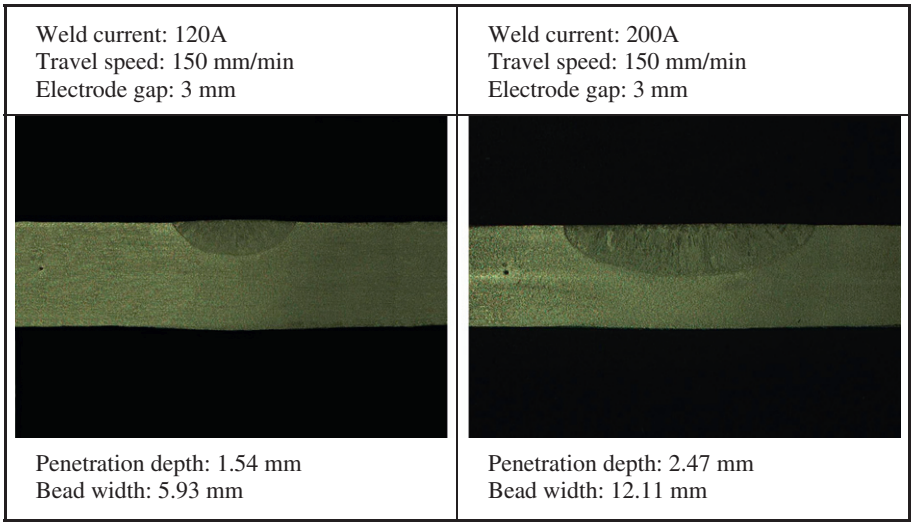

Fig. 7. Comparison of current levels on geometric shape of conventional TIG welds.

3.3. Geometric shape of activated TIG welds

Fig. 9 presents a transverse cross-section of stainless steel TIG welds produced without and with flux powder. Fig. 9a and b show the results of TIG welding without flux powder and with FeF_2 powder, which produced a shallow, wide profile. Fig. 9c and d show that FeO and FeS powders produced a deep, narrow profile. In this experiment, FeO powder facilitated complete penetration in austenitic 316 L stainless steel TIG welds. Thus, the FeO and FeS powders are capable of increasing the depth-to-width (aspect) ratio of TIG welds. A weld with a high aspect ratio indicates increased energy density of the heat source in welding, which produces a high concentration of heat energy during welding. As the energy density of the heat source increases, the overall heat required per unit length of the weld decreases. Thus, activated TIG welding is considered a higher energy density process. In addition, the ability of the heat source to melt the base metal is a matter of practical interest in TIG welding. At the same weld current and travel speed, activated TIG welding can increase the deposition rate of the welds. This indicates that activated TIG welding also achieves higher melting efficiency. The benefit of using activated flux in conventional TIG welding is a significant reduction in the amount of arc heat required for the welds with a large cross-sectional area and a high joint penetration.

This experiment also found that using FeS powder resulted in undercut (Fig. 9d). Undercut is an appearance defect that appears as a jagged groove melted into the base metal adjacent to the toe of weld and left unfilled by weld metal. Previous research has reported that the undercut at the weld toe is the most significant geometric effect affecting the fatigue behavior of the butt-welded joints [16]. For this reason, undercut defect should be avoided.

3.4. Mechanisms underlying increased penetration capability of activated TIG welds

The variable depth of penetration can be attributed to surface-active trace elements, which cause changes in the weld pool flow in response to the surface tension gradient. This effect is called the Marangoni convection. Oxygen and sulfur are the surface-active trace elements most commonly found in iron-based alloys. In TIG welding without flux powder, the temperature dependence of surface tension in a molten weld pool generally exhibits a negative value (Fig. 10a). In this case, the surface tension in the center of the weld pool is lower than that around the edge of the weld pool. The resulting negative surface tension gradient causes a centrifugal Marangoni convection (Fig. 10b). Under this condition, the fluid flow of the molten weld pool is transferred from the center of the weld pool to the edges, resulting in a wide, shallow weld (Fig. 9a). Heiple et al. suggested that small concentrations of particular surface-active trace elements in a molten weld pool can convert the temperature dependence of surface tension from a negative to positive value (Fig. 10c). In TIG welding with FeO and FeS powders, the surface tension in the center of the weld pool exceeds that of the edges, thereby reversing the surface tension gradient. A positive surface tension gradient causes a centripetal Marangoni convection (Fig. 10d). Under this condition, the fluid of a molten weld pool flows from the edge of the weld pool to the center and then downward, resulting in a deep, narrow weld (Fig. 9c and d). Previous research has reported that the surface tension of molten fluorides indicates a negative linear relationship with temperature [17]. In TIG welding with FeF_2 powder, a Marangoni convection creates the same centrifugal pattern found in TIG welding without flux powder, which has unfavorable effects on the penetration improvement (Fig. 9b).

Consensus is lacking on the mechanism by which flux powder increases the penetration of TIG welds. For a theoretical consideration of the possible mechanisms, this study suggests that the redistribution of conduction electrons may account for the physics involved in arc columns. An arc is an electric discharge between an anode and a cathode, and this discharge passes through extremely ionized gas known as arc plasma. The arc discharge channel between two electrodes can be conveniently divided into three regions: a central region or arc column, in which there is a uniform potential gradient, and two regions adjacent to the electrodes, in which the cooling effect of electrodes causes a potential drop. These two regions are known as the anode and cathode drop regions, depending on the direction of current flow.

An arc column comprises two concentric zones: an inner core, called the arc plasma, and an outer flame. The arc plasma carries the electric current and has the highest temperature. The outer flame is substantially cooler and tends to hold the arc plasma within the central zone. Compared to TIG welding without flux powder, the arc

Table 3
Process parameter of activated TIG welding experiments.

Weld current	170 A
Travel speed	150 mm/min
Electrode gap	3 mm
Shielding gas	Argon
gas flowrate	12 L/min

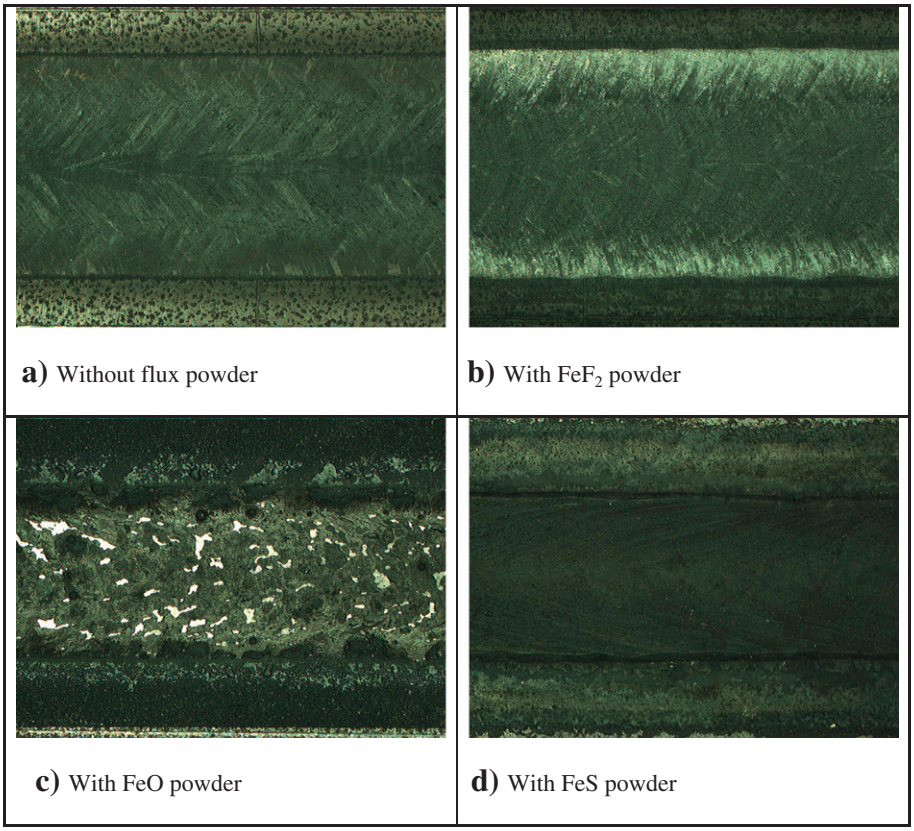

Fig. 8. Effect of TIG welding with various flux powders on surface appearance.

column of TIG welding with FeO and FeS powders is clearly constricted (Fig. 11). The degree to which the arc column is constricted is related to the ability of dissociated atoms to capture additional electrons. The ionization potential is the energy required to completely remove an electron from an atom, a molecule, or an ion. The closer and more tightly bound an electron is to the nucleus, the more difficult it is to remove, and the higher its ionization potential will be. In the inner region of the arc column, the temperature of the arc plasma is substantially higher than the ionization temperature of the flux powders. Thus, the ionized atoms of the flux powders are more likely to generate free electrons and positive ions. In a state of complete ionization, electrons in the plasma have much greater mobility than the ions. Therefore, the electric current is almost entirely due to the flow of electrons. In the outer region of the arc column, vaporized compounds still exist as molecules and dissociated atoms. When the free electrons come into contact with the dissociated atoms, the atoms attract the electrons, forming negative ions. Consequently, this reduces the number of free electrons in the outer region of the arc column. This constricts the arc column to a local self-equilibrium condensed state. As Table 2 shows, the ionization potential of FeO and FeS powders is substantially lower than that of FeF_2 powder, which promotes the capture of free electrons in the outer region of the arc column. Consequently, the arc column of TIG welding with FeO and FeS powders is considerably constricted.

Fig. 12 shows the influence of various flux powders on arc voltage. Results indicate that FeO and FeS powders increased the arc voltage during welding, but FeF_2 powder has little effect on the arc voltage. Because the arc column is constricted, the conducting channel of the arc current decreased. Consequently, the arc voltage of TIG welding with FeO and FeS powders must be increased to maintain arc current continuity in the arc column during welding. There is a clear correlation between the measured arc voltage and the observed arc constriction (i.e., increasing the arc voltage increases the constriction of the arc column).

In TIG welding with FeO or FeS powder, the constricted arc column increases the energy density of heat source, generating a high current density at the surface of molten weld pool. The resulting large Lorentz force and a high arc pressure contribute a forceful downward flow of heat in molten weld pool. Moreover, the inward radial flow of the centripetal Marangoni convection (caused by the oxygen and sulfur elements in the FeO and FeS compounds, respectively) further promotes the transfer of arc heat from the surface to the bottom of the molten weld pool. As a result, the interaction effect between the constricted arc column and the centripetal Marangoni convection significantly increase the penetration depth and reduce the bead width. However, TIG welding with FeF_2 powder appears to have little effect on either the chemistry of molten weld pool or the physics of the arc column, and thus, does not promote an increase in weld aspect ratio. Fig. 13 illustrates a summary of the mechanisms underlying the increased penetration capability of TIG welding with various flux powders.

3.5. Angular distortion of activated TIG welds

Because austenitic stainless steels have a higher thermal expansion and a lower thermal conductivity than plain carbon steels, they are subject to greater shrinkage or distortion after welding. Determining the influence of flux powders on thermal distortion is essential to improving the performance of the stainless steel activated TIG weldment. Angular distortion often occurs in a weldment when non-uniform thermal shrinkage in the direction normal to the surface changes the angle close to the weld line. The angular distortion of the weldment depends on several factors, including the penetration depth to plate thickness ratio, and the shape and dimensions of the welds. The energy density of the heat source is another important factor influencing the angular distortion of the weldment because it directly determines the geometric shape of TIG welds.

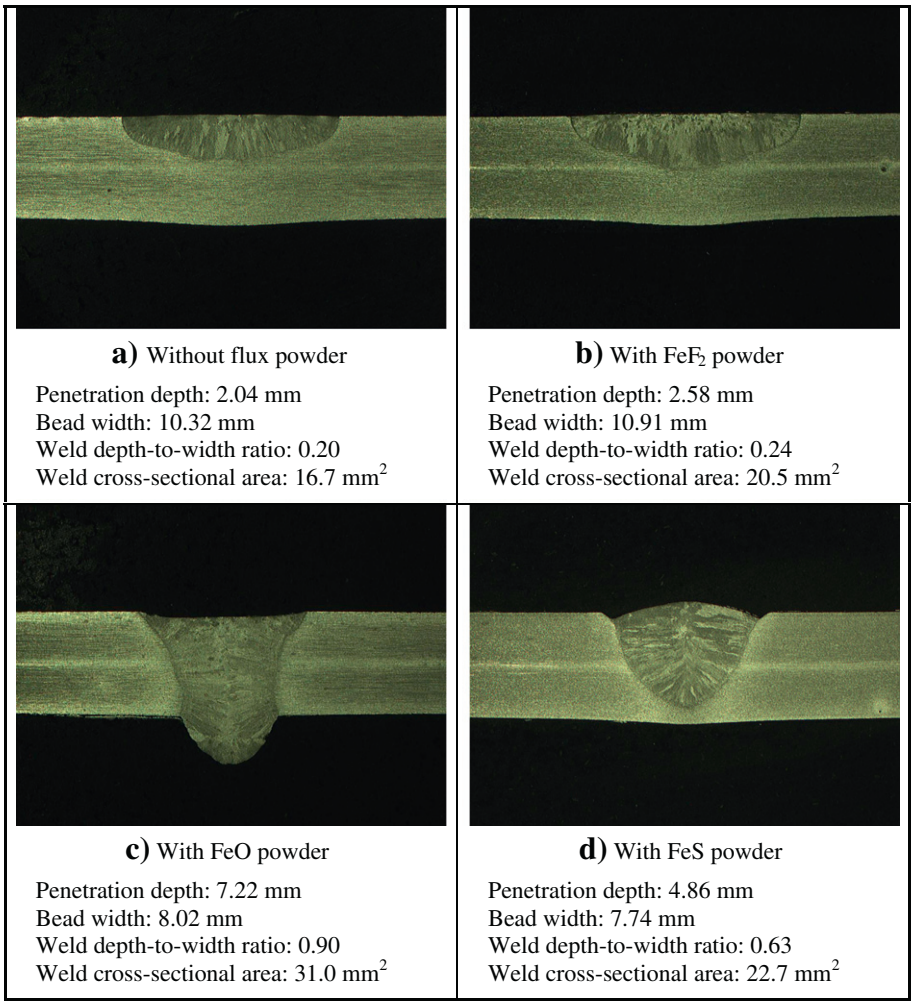

Fig. 9. Effect of TIG welding with various flux powders on geometric shape.

This study expresses angular distortion for total angular changes in the weldment. Fig. 14 shows the angular distortion of the TIG weldment produced without and with flux powder. Results indicate that activated TIG welding significantly reduces the angular distortion of the weldment. As mentioned, an activated TIG welding produces a substantial increase in both the penetration depth and weld aspect ratio, which is a characteristic of high energy density heat source. This reduces the quantity of supplied arc heat, which consequently

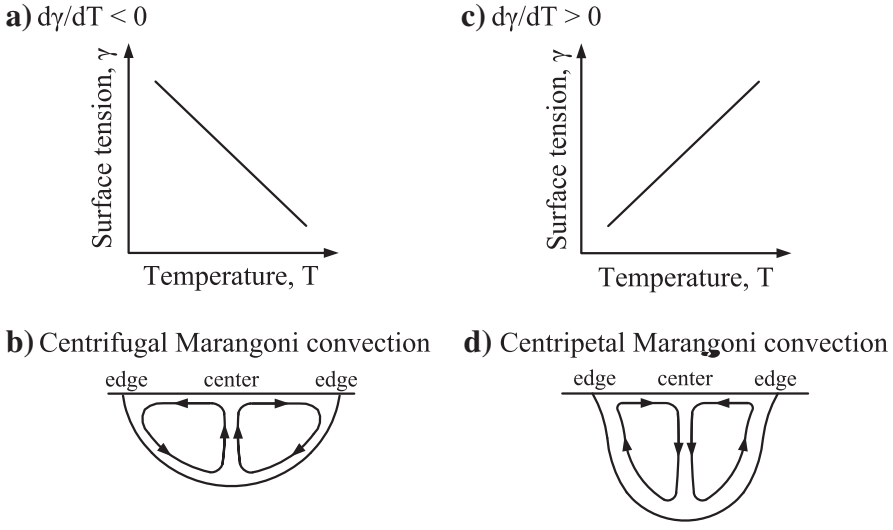

Fig. 10. Fluid flow pattern for molten weld pool.

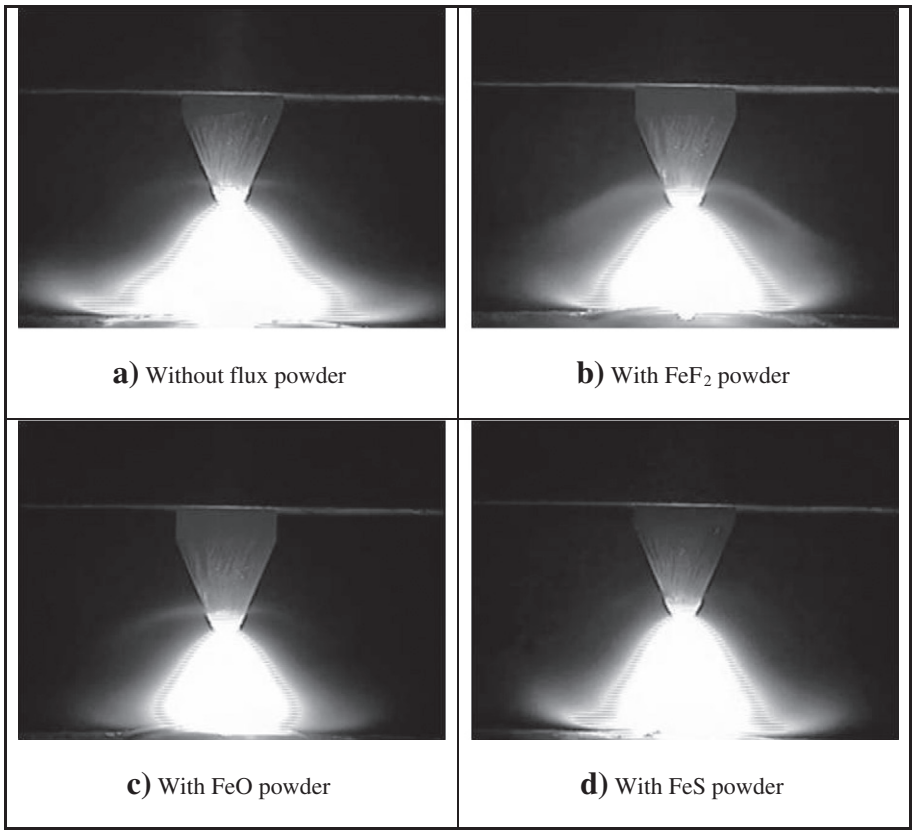

Fig. 11. Comparison of arc column of TIG welding with various flux powders.

prevents overheating of the weldment and reduces the incidence of thermal stress and incompatible strain caused by shrinkage in the through-thickness direction of the weldment. As a result, the angular distortion of the activated TIG weldment can be reduced. TIG welding with FeO powder provides the greatest penetration depth and weld aspect ratio, significantly reducing the angular distortion.

3.6. Metallurgical properties of activated TIG welds

To determine the phase constitution after welding, the weld metal of 17Cr–10Ni–2Mo alloy is analyzed by means of X-ray diffraction (XRD) technique using a Cu target operated at 40 kV and 40 mA. The data were collected in the 2θ range of 35–95° at a scan rate of 5°/min. Fig. 15 shows the experimental XRD pattern. Results show that the phase within the weld metal exhibits a duplex structure consisting of bcc ferrite (JCPDS No. 06-0696) and fcc austenite (JCPDS No. 31-0619). Fig. 16 shows a SEM photograph of microstructure for 17Cr–10Ni–2Mo alloy TIG welds; it reveals the discontinuous skeletal delta-ferrite (δ) structures in a predominant austenite matrix. The delta-ferrite of a duplex structure, which forms as a result of rapid solidification, is usually a metastable phase at temperatures below 1000 °C [18]. Fig. 17 shows the delta-ferrite content of the TIG weld metal produced without and with flux powder. The experiments in this study used hot-rolled austenitic 316 L stainless steel plate with an average of 0.7 FN as a base metal. In TIG welding without flux powder, the measured delta-ferrite content in weld metal averaged 5.3 FN. During welding, the cooling rate of the weld metal is so rapid that the phase transformation of delta-ferrite to austenite remains incomplete. Consequently, an austenite matrix contains more delta-ferrite structure after cooling and solidification from the molten state.

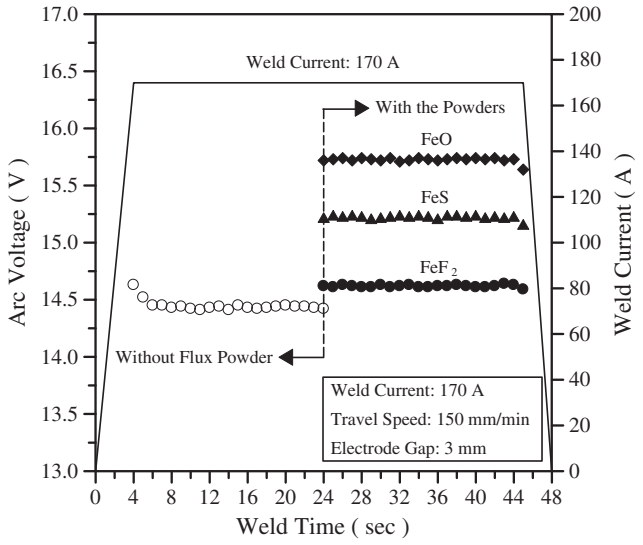

Fig. 12. Effect of TIG welding with various flux powders on arc voltage.

TIG welding with FeF_2 powder has no effect on the delta-ferrite content of weld metal, which showed an average of 5.8 FN. In TIG welding with FeO and FeS powders, the measured delta-ferrite content increased to 8.1–8.5 FN. This increase is directly related to the total heat input required to produce a weld. Because a higher heat input can increase the peak temperature of the weld metal and reduce its cooling rate. In other words, the most important characteristic of heat input is how it influences the cooling rate in weld metal, thereby affecting metallurgical structures. TIG welding with FeO or FeS powder has a high energy density heat source, which is characterized by a low heat input and consequently rapid cooling rate. The rapid cooling rate of TIG welding with FeO or FeS powder leads to an incomplete transformation of the delta-ferrite phase to the austenite phase as the weld metal solidifies. In this case, the weld metal

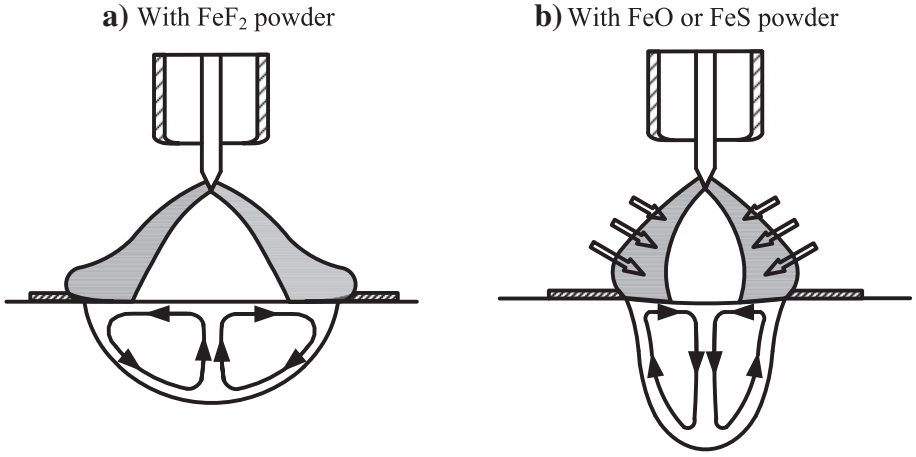

Fig. 13. Schematic diagram of mechanism for increased penetration of activated TIG welds.

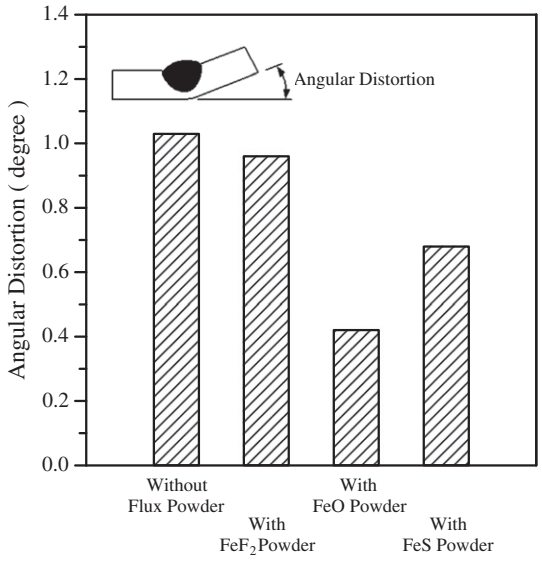

Fig. 14. Effect of TIG welding with various flux powders on angular distortion.

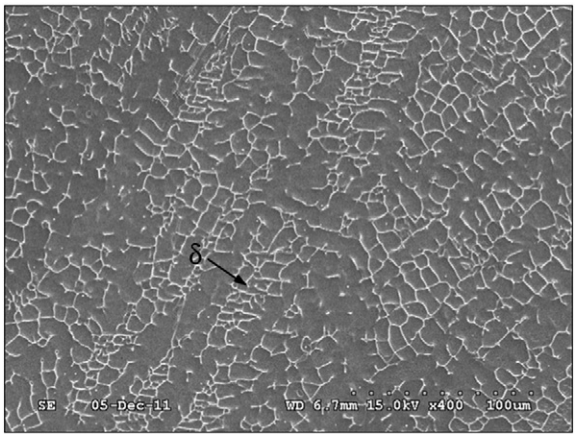

Fig. 16. SEM photograph of microstructure for 17Cr–10Ni–2Mo alloy weld metal.

retains a higher percentage of metastable delta-ferrite at room temperature.

Fig. 18 presents the hardness distribution profile of TIG weldments produced without and with flux powder. Results show that

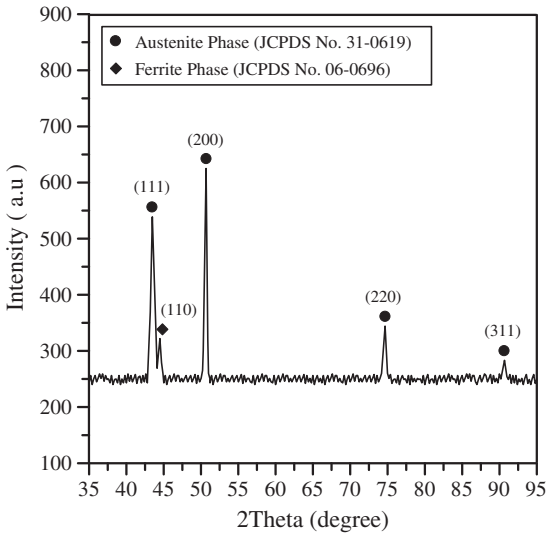

Fig. 15. XRD pattern of weld metal for 17Cr–10Ni–2Mo alloy.

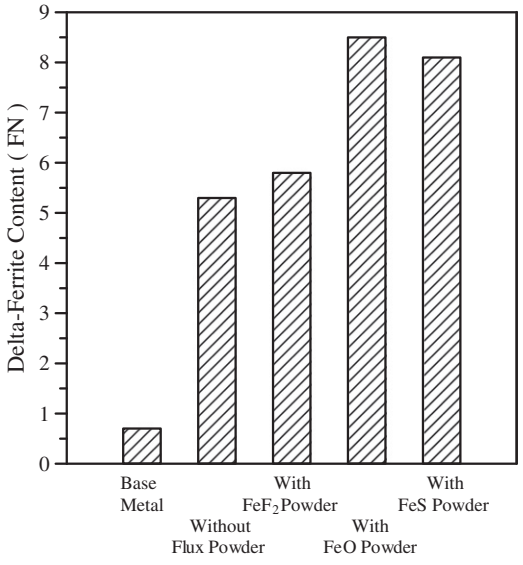

Fig. 17. Effect of TIG welding with various flux powders on delta-ferrite content.

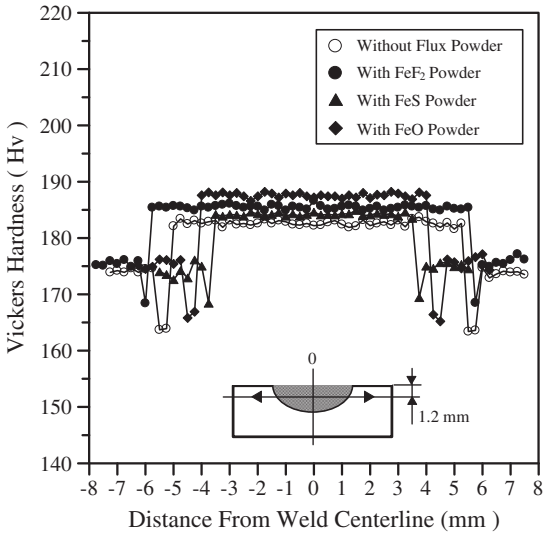

Fig. 18. Effect of TIG welding with various flux powders on hardness distribution profile.

weld metal has the highest hardness, whereas the HAZ has a lower hardness than the base metal. TIG welding without flux powder or with various flux powders increases the delta-ferrite content in weld metal, which in turn increases the hardness of the welds. The hardness profiles of the weldment do not change significantly when flux powder is used in the TIG welding process.

3.7. Hot crack susceptibility of activated TIG welds

Calculating the crack lengths in both the FZ and HAZ makes it possible to evaluate the hot crack susceptibility of the welds. The total and maximum crack lengths were measured on the specimen surface using a high-resolution digital camera, and the resulting images were viewed on a PC at high magnification. Fig. 19 shows the hot crack morphology of the welds produced without and with flux powder. Results show a reduction in measured total and maximum crack lengths when using the activated TIG welding process. This study proposes two explanations to explain the beneficial effects of activated TIG welding technique in reducing the hot crack susceptibility of the 17Cr–10Ni–2Mo alloy TIG welds. The first explanation is that the high-temperature ductility of the delta-ferrite phase exceeds that of the austenite phase. Therefore, the delta-ferrite structure within an austenite matrix can reduce thermal shrinkage stress during welding [19]. The second explanation is that the amount of heat input per unit length in an activated TIG weld is lower than that of the conventional TIG welds, and thereby reduces the tensile residual stress during cooling [20]. When FeO and FeS powders are used in the TIG welding technique, the delta-ferrite content in weld metal increases and requires welding heat input decreases, therefore has a beneficial effect in reducing the hot crack susceptibility.

4. Conclusions

The experiments reported in this study used FeF_2, FeO, and FeS as flux powders and investigated their effects on the surface appearance, geometric shape, angular distortion, hot crack susceptibility, and

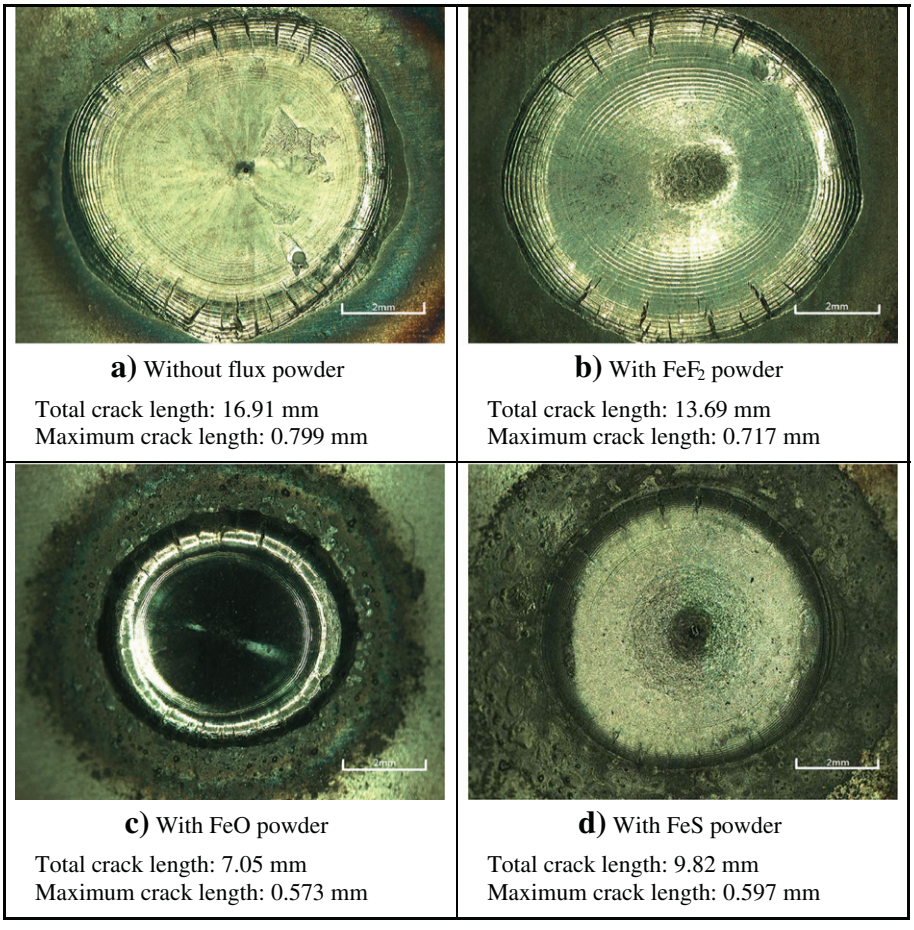

Fig. 19. Effect of TIG welding with various flux powders on hot crack susceptibility.

metallurgical properties of the TIG welds. The following points summarize the experimental results:

1. TIG welds produced with FeF_2 powder had a satisfactory surface appearance, whereas the FeO and FeS welds produced slag and spatter. Unfortunately, TIG welding with FeS powder resulted in undercut.
2. TIG welding with FeO and FeS powders increases both the joint penetration and weld aspect ratio, reducing the angular distortion.
3. TIG welding with FeO and FeS powders increases the delta-ferrite content and decreases the welding heat input, and tends to reduce the hot crack susceptibility.
4. TIG welding with FeO and FeS powders, the multiplication effect between the constricted arc column and the centripetal Marangoni convection increases the penetration depth and reduces the bead width. However, TIG welding with FeF_2 powder appears to have little effect on either the chemistry of the weld pool or the physics of the arc column, and does not significantly increase the weld aspect ratio.
5. The FeO powder assisted TIG welding can obtain deep penetration, low distortion, and satisfactory performance for the 17Cr–10Ni–2Mo alloys.

Acknowledgements

The authors gratefully acknowledge the financial support provided to this study by the National Science Council under the grant no. 100-2221-E-020-012 and the Ministry of Economic Affairs under the grant no. 98-EC-17-A-16-S1-121, Taiwan. In this experimental work, SEM was performed in the Precision Instruments Center of NPUST.

References

[1] P.J. Modenesi, E.R. Apolinario, I.M. Pereira, TIG welding with single-component fluxes, Journal of Materials Processing Technology 99 (2000) 260–265.
[2] H.Y. Huang, S.W. Shyu, K.H. Tseng, C.P. Chou, Evaluation of TIG flux welding on the characteristics of stainless steel, Science and Technology of Welding and Joining 10 (5) (2005) 566–573.
[3] S.W. Shyu, H.Y. Huang, K.H. Tseng, C.P. Chou, Study of the performance of stainless steel A-TIG welds, Journal of Materials Engineering and Performance 17 (2) (2008) 197–201.
[4] T.S. Chern, K.H. Tseng, H.L. Tsai, Study of the characteristics of duplex stainless steel activated tungsten inert gas welds, Materials and Design 32 (1) (2011) 255–263.
[5] K.H. Tseng, C.Y. Hsu, Performance of activated TIG process in austenitic stainless steel welds, Journal of Materials Processing Technology 211 (2011) 503–512.
[6] S. Leconte, P. Paillard, P. Chapelle, G. Henrion, J. Saindrenan, Effects of flux containing fluorides on TIG welding process, Science and Technology of Welding and Joining 12 (2) (2007) 120–126.
[7] C.H. Kuo, K.H. Tseng, C.P. Chou, Effect of activated TIG flux on performance of dissimilar welds between mild steel and stainless steel, Key Engineering Materials 479 (2011) 74–80.
[8] S.M. Gurevich, V.N. Zamkov, N.A. Kushnirenko, Improving the penetration of titanium alloys when they are welded by argon tungsten arc process, Avtomaticheskaya Svarka 9 (1965) 1–4.
[9] C.R. Heiple, J.R. Roper, Effect of selenium on GTAW fusion zone geometry, Welding Journal 60 (8) (1981) 143–145.
[10] C.R. Heiple, J.R. Roper, Mechanism for minor element effect on GTA fusion zone geometry, Welding Journal 61 (4) (1982) 97–102.
[11] C.R. Heiple, J.R. Roper, R.T. Stagner, R.J. Aden, Surface active element effects on the shape of GTA, Laser, and electron beam welds, Welding Journal 62 (3) (1983) 72–77.
[12] C.R. Heiple, P. Burgardt, Effects of SO_2 shielding gas additions on GTA weld shape, Welding Journal 64 (6) (1985) 159–162.
[13] P. Burgardt, C.R. Heiple, Interaction between impurities and welding variables in determining GTA weld shape, Welding Journal 65 (6) (1986) 150–155.
[14] W. Lucas, D. Howse, Activating flux- increasing the performance and productivity of the TIG and plasma processes, Welding and Metal Fabrication 64 (1) (1996) 11–17.
[15] D.S. Howse, W. Lucas, Investigation into arc constriction by active fluxes for tungsten inert gas welding, Science and Technology of Welding and Joining 5 (3) (2000) 189–193.
[16] N.T. Nguyen, M.A. Wahab, The effect of undercut and residual stresses on fatigue behaviour of misaligned butt joints, Engineering Fracture Mechanics 55 (3) (1996) 453–469.
[17] A. Ejima, M. Shimoji, Effect of alkali and alkaline-earth fluorides on surface tension of molten calcium silicates, Transactions of the Faraday Society 66 (1970) 99–106.
[18] M. Martins, L.C. Casteletti, Sigma phase morphologies in cast and aged super duplex stainless steel, Materials Characterization 60 (8) (2009) 792–795.
[19] K.H. Tseng, C.P. Chou, The study of nitrogen in argon gas on the angular distortion of austenitic stainless steel weldments, Journal of Materials Processing Technology 142 (2003) 139–144.
[20] K.H. Tseng, Y.C. Chen, K.L. Chen, Cr_2O_3 flux assisted TIG welding of type 316L stainless steel plates, Applied Mechanics and Materials 121–126 (2012) 2592–2596.